Integrated Coherent Tunable Laser (ICTL) With Ultra-Wideband Wavelength Tuning and Sub-100 Hz Lorentzian Linewidth

Paul A. Morton, *Fellow, IEEE*, Chao Xiang, Jacob B. Khurgin, *Fellow, IEEE*, Christopher D. Morton, Minh Tran, Jon Peters, Joel Guo, Michael J. Morton, and John E. Bowers, *Fellow, IEEE*

(Top-Scored Paper)

***Abstract*—This paper describes the design, fabrication, and record performance of a new class of ultra-wideband wavelength tuning, ultra-low noise semiconductor laser, the Integrated Coherent Tunable Laser (ICTL). The ICTL device is designed for, and fabricated in, a CMOS foundry based Silicon Photonics platform, utilizing heterogeneous integration of III-V material to create the integrated gain section of the laser–enabling high-volume mass-market manufacturing at low cost and with high reliability. The ICTL incorporates three or more ultra-low loss micro-ring resonators, with large ring size, in a Sagnac loop reflector geometry, creating exceptional laser reflector performance, plus an extended laser cavity length that enables highly-coherent output; ultra-low linewidth and phase noise. This paper describes record integrated laser performance; 118 nm wavelength tuning, covering S-, C- and L-bands, with Lorentzian linewidth $<$100 Hz, and with excellent relative intensity noise (RIN) of ≤ -155 dBc/Hz. The remarkable performance of the ICTL device, coupled with the high volume/low cost capability of the Silicon Photonics platform enables next-generation applications including ultra-wideband WDM transmission systems, fiber-optic and medical-wearable sensing systems, and automotive FMCW LiDAR systems utilizing wavelength scanning.**

***Index Terms*—Heterogeneous integration, laser tuning, low relative intensity noise, narrow linewidth, semiconductor laser, silicon photonics, ultra-low noise, ultra-wideband wavelength tuning.**

I. Introduction

HIGH-PERFORMANCE lasers are key components for a wide range of communications, sensing, and RF photonics applications. Extremely low Frequency Noise (FN) is important for coherent systems using advanced modulation formats (e.g., higher order QAM), where signal and optical local oscillator are mixed in photodetectors to provide electrical outputs, and in RF photonics where two optical signals mix in a photodetector to produce an RF signal [1]. Optical sensing systems including FMCW LiDAR, distributed fiber sensing, and interferometric acoustic sensing systems also require extremely small low-frequency FN and associated ultra-low Lorentzian linewidth. Applications currently dominated by expensive, bulky, power-hungry solid state and fiber lasers can now be addressed by integrated, ultra-low linewidth semiconductor lasers with the benefits of reduced size, weight, power consumption and cost (SWaP-C). In addition, many applications require lasers that operate over a wide wavelength range, e.g., ultra-wide band (UWB) wavelength division multiplexed (WDM) systems operating across S-, C- and L-Bands [2], or in systems leveraging ultra-wideband wavelength tunability, e.g., automotive LIDAR using wavelength for scanning [3], where the wavelength tuning range is paramount. This paper describes a laser design that addresses all of these requirements; high power, ultra-low FN and Lorentzian linewidth, ultra-wideband wavelength tuning, and extremely low relative intensity noise (RIN) [4]. The Integrated Coherent Tunable Laser (ICTL) device is developed on a CMOS Foundry compatible Silicon Photonics platform that is enabled by heterogeneous integration [5], to create a high-volume, low-cost, integrated laser with unparalleled performance, that will be disruptive in many applications [6].

Manuscript received July 5, 2021; revised September 16, 2021 and October 17, 2021; accepted November 3, 2021. Date of publication November 10, 2021; date of current version March 16, 2022. This research of paper was performed under Contract W911NF-16-C-0072 with the Defense Advanced Research Projects Agency (DARPA). *(Corresponding author: Paul A. Morton.)*

Paul A. Morton, Christopher D. Morton, and Michael J. Morton are with Morton Photonics Inc., West Friendship, MD 21794 USA (e-mail: pmorton@mortonphotonics.com).

Chao Xiang, Jon Peters, Joel Guo, and John E. Bowers are with the University of California, Santa Barbara, CA 93106 USA (e-mail: bowers@ece.ucsb.edu).

Jacob B. Khurgin is with the Johns Hopkins University, Baltimore, MD 21218 USA.

Minh Tran is with Nexus Photonics, Santa Barbara, CA 93117 USA.

Color versions of one or more figures in this article are available at https://doi.org/10.1109/JLT.2021.3127155.

Digital Object Identifier 10.1109/JLT.2021.3127155

II. ICTL Design

The novel ICTL device design is a new approach for micro-ring resonator (MRR) based tunable lasers; it is not just a simple extension of a vernier tuned two MRR based laser, made by adding a third tuning MRR. Ultra-wide wavelength tuning together with ultra-low noise performance, i.e., linewidth and RIN, require a long, low-loss external cavity – therefore made of ultra-low loss (ULL) waveguides, in addition to excellent laser cavity singlemode selectivity, i.e., a high suppression of unwanted laser modes. Typical two MRR based integrated tunable lasers use vernier tuning; i.e., two MRRs designed with as small a radius/circumference as possible in order to expand the tuning

range while still ensuring singlemode operation, e.g., [7]–[11]. This compromise approach limits the potential tuning range as well as the laser performance, because small MRRs require tight optical confinement for low bending losses in the small radius rings, leading to designs with high waveguide losses and shorter effective cavity lengths – and therefore larger linewidth. Additionally, the use of high Q MRRs to increase the effective cavity length also increases the power density in the MRR and therefore can increase nonlinear loss. This is particularly important in Silicon Photonics foundry based devices using silicon waveguides, due to two photon absorption (TPA) and associated free carrier absorption (FCA) in the waveguides [12], which further increases MRR losses. Conversely, the ICTL utilizes three or more MRRs fabricated from ULL waveguides and large circumference MRRs [15], in order to meet all of these requirements, without compromise. Extensive numerical simulations are required in order to create the optimum ring-based laser reflector designs, to meet all the performance goals, with all ICTL designs in this paper being carried out using a GUI based laser reflector optimization tool.

The ICTL device is designed to include a specific external cavity reflection design, initially modeled on the fiber Bragg grating (FBG) based extended-distributed Bragg reflector (E-DBR) laser product developed by Morton Photonics, which can produce Lorentzian linewidths as low as 15 Hz [13]. A commercial version of the FBG based E-DBR laser provides 150 mW output power at 1550 nm, Lorentzian linewidth below 100 Hz, and RIN below −165 dBc/Hz [14].

While the laser reflector design for the ICTL was initially modeled on a custom high-performance FBG design, it is notable that the limitations of even the best/optimally written FBGs can be improved upon by using an MRR based reflector. Additionally, an MRR based reflector can typically provide wide wavelength tunability, by tuning the ring resonance frequencies – requiring more complex control, whereas grating based lasers are usually single wavelength devices. FBGs can provide a narrow reflection peak, with long associated cavity length, however, due to laser design and FBG writing, practical gratings will have sidelobes that affect the laser performance. This can be overcome in an MRR based laser reflector that uses lithography to control coupling coefficients on each side of the MRR, and the length of the ring. The ring circumference (optical length) is the key parameter, and this can be varied by changing the temperature of the waveguide using the thermo-optic effect, varying effective optical length and the ring resonance frequencies as a result. Fluctuations in temperature across the device can be counteracted by tuning the overall length of the MRR to its desired value, while temperature variations along a grating cannot be so easily counteracted.

A schematic of a three ring ICTL device is shown in Fig. 1. The gain section can be a silicon rib waveguide with III-V material bonded on top to provide a III-V/Si hybrid waveguide [5], or a III-V gain chip heterogeneously integrated by die attach or by micro-transfer printing [16]. The gain section is coupled to an external cavity (right) including a phase control element, a 2:2 tunable coupler (50/50), which, when combined with the three rings interconnected by bus waveguides, forms the laser reflector (in blue). The laser reflector is a Sagnac loop

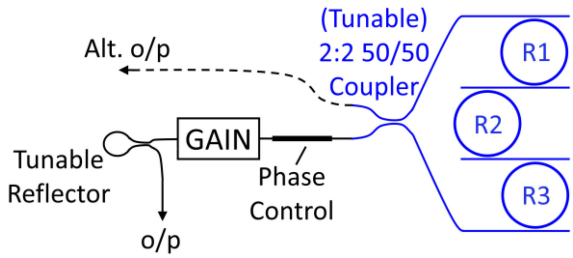

Fig. 1. Schematic of a 3 ring ICTL device: A III-V heterogeneously integrated gain element, a tunable loop reflector forming one laser cavity end, and an ultra-wideband wavelength tunable laser reflector incorporating three large bus-coupled microresonators in a Sagnac loop configuration forming the other laser reflector. A phase control element controls the laser cavity mode.

mirror that incorporates three or more MRRs interconnected by bus waveguides, and with the coupler set at 50/50 then 100% of the reflection goes back to the gain chip. The tunable 2:2 coupler allows the 50/50 coupling ratio to be achieved over the full (ultra-wide) wavelength operating range of the ICTL. The alternative output of the 2:2 coupler can be used to optimize the coupler splitting ratio, e.g., measuring power on an integrated photodetector, and minimizing this output would maximize the power back to the gain chip. Additionally, this alternative output can be used as the main output of the laser, by changing the coupling ratio to direct part of the output to it. In this case, the reflector on the left side of the gain element would be set to maximum reflectivity, approaching 100%, and the laser output taken from the alternative output. An advantage of using this alternative output is that the optical power has just passed through the laser reflector, which filters amplified spontaneous emission (ASE) noise away from the lasing wavelength, further reducing the laser RIN. The 'standard' output taken from the left end of the gain element includes additional ASE noise from a pass through the gain element.

A tunable loop reflector can be used on the left side of the gain element to provide the left end of the laser cavity as well as to provide the optical output. This provides the desired optical feedback while being an easy element to include on an integrated platform with other components on a photonic integrated circuit (PIC), such as a modulator, and allows the reflectivity of that end of the laser cavity and the output power to be optimized.

The design and operation of the three ring laser reflector is explained through the reflection spectra shown in Figs. 2 and 3. It is most easily understood by starting with the reflection spectrum from a single MRR based laser reflector, as shown in Fig. 2a. The single ring provides a constant peak amplitude comb of reflections with an FSR given by the circumference, L, of the ring ($FSR = c/n_{eff}.L$), where n_{eff} is the effective index of the MRR ring waveguide. For the ICTL device described in this paper, this first Si ring has a radius of 599.967 μm (close to the 600 μm minimum radius for ultra-low-loss Si MRR operation), for an FSR of 22.1 GHz with a group index 3.6064. The bandwidth of each of these reflections is 0.74 GHz, the time delay/effective length of the ring is 409 ps. A second ring is added to the first, with a radius slightly larger than the first (600.856 μm), providing the broad reflection spectrum shown in Fig. 2b. The super-structure repeat reflection peaks are seen near 1440 nm

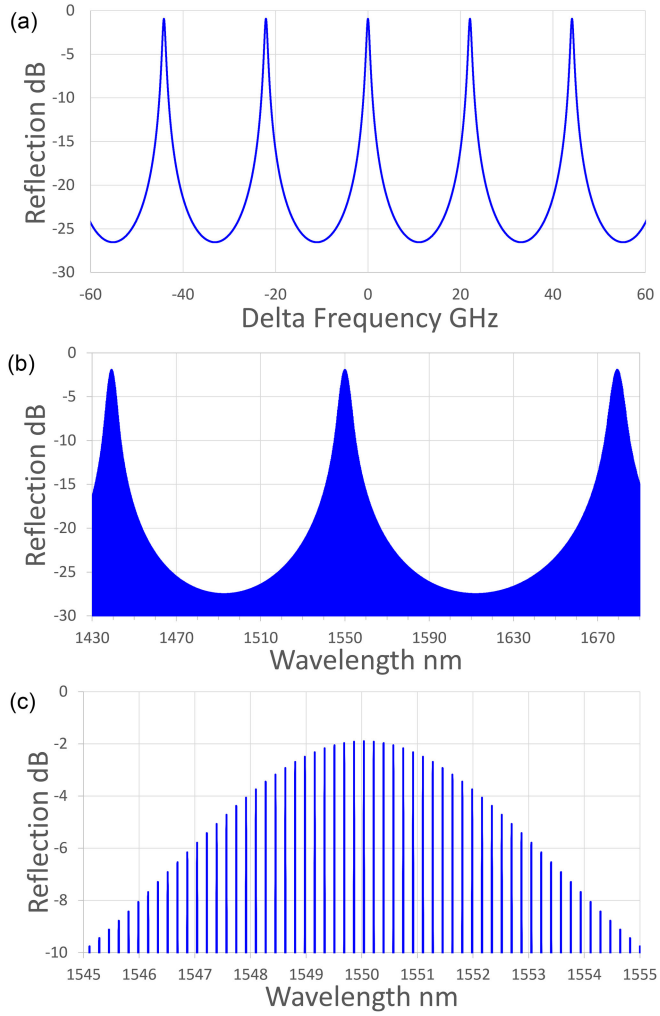

Fig. 2. Laser reflector reflection spectra; a) Single Ring (radius 599.967 μm), and Dual Ring (600.856 μm), on b) wide, and c) narrow wavelength ranges.

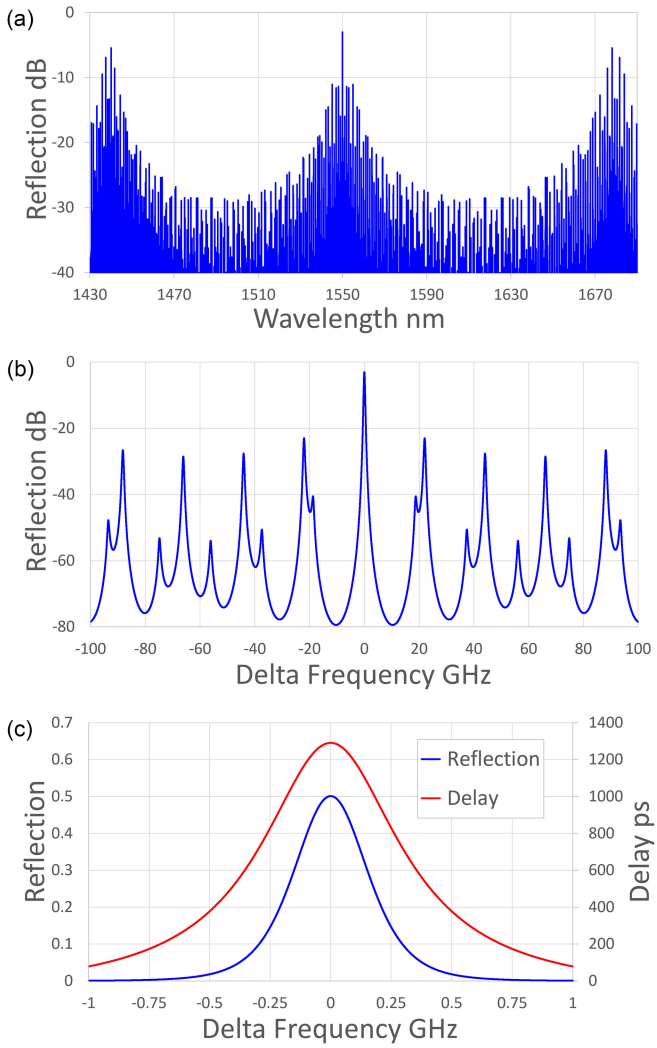

Fig. 3. Three Ring laser reflector spectra; a) wide, b) close (+/− 100 GHz), and c) showing linear reflection central peak, and group delay.

and 1680 nm, providing a total tuning range of (1680-1440)/2, i.e., 120 nm. However, looking close in at the reflection peak near 1550 nm (Fig. 2c) there are still many reflection peaks with similar peak reflectivity, and the dual ring reflector therefore cannot support single mode laser operation.

The ICTL design process then adds a third ring, this radius is chosen to provide the optimum laser reflector response, i.e., excellent singlemode selectivity over a very wide tuning range, as well as a high tolerance to potential variations from device fabrication. This design process is carried out using a custom Matlab based laser reflector simulation and optimization tool. Results for the device demonstrated in this paper are shown in Fig. 3. The wide reflection response in Fig. 3a shows that all potential lasing modes over 120 nm tuning range (before the next super-structure peaks) are $\geq$8.4 dB lower than the main reflection peak. As part of the design process more significance is placed on close in reflection peaks, i.e., +/− 100 GHz from the central peak, shown in Fig. 3b, as these have more impact on lasing operation and noise, and in this case, all of the close in reflection peaks are at least 20 dB lower than the main peak.

The laser reflector has a peak amplitude reflectivity of 0.5, assuming a ULL Si loss of 0.25 dB/cm, and for a design with a coupling coefficient (κ) between each ring and bus waveguide of 0.3 (amplitude). The effective length of this laser reflector is 108 mm (1.3 ns group delay), enabling the record narrow linewidths but also explaining how sensitive the device is to ULL Si waveguide loss. The laser reflector has a design FWHM of 0.36 GHz.

Initial laser reflectors were designed and fabricated using Si_3N_4 ULL waveguides and excellent performance was shown [17]; a three ring laser reflector using pulley couplers provided 15 dB suppression of all reflector sidelobes over the full measurement range of 80 nm, whereas a four ring laser reflector design provided additional sidelobe suppression of 20 dB. Adding an additional ring (or more) provides additional degrees of freedom in the ICTL design, allowing the laser reflector and ICTL performance to be optimized for a specific application. E-DBR lasers incorporating a Si_3N_4 Bragg reflector and using a multilayer heterogeneous integration approach to add the III-V gain element have been demonstrated [18], [19]. This process is

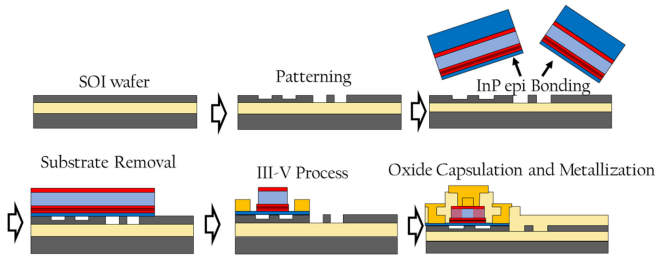

Fig. 4. UCSB Silicon Photonics Heterogeneous Integration process flow.

being extended in order to create the first Si_3N_4 laser reflector based ICTL devices.

With the development of ULL silicon waveguides as part of the UCSB heterogeneous silicon photonics platform [20], which provide singlemode passive waveguide loss as low as 0.16 dB/cm, fully integrated E-DBR lasers with III-V on silicon hybrid gain elements and ULL Si Bragg gratings were demonstrated [21]. Low loss and higher optical power handling capability could be provided by a multi-micron Si waveguide platform [22]. Early ICTL devices using ULL silicon waveguides showed encouraging results [23] by taking advantage of large (600 μm) MRRs with low waveguide loss, however, processing issues from wafer bonding and high P-contact resistance required excessive anneals that damaged the gain sections, leading to low optical power and degradation during testing. New processes have been developed to overcome these limitations, leading to the ICTL devices described in this paper.

III. Heterogeneous Silicon Photonics Fabrication

ICTL devices were fabricated on the UCSB heterogeneous silicon photonics platform [5]; the main process sequence is shown in Fig. 4. SOI wafers with a 500 nm Si device layer and 1 μm bottom oxide (BOX) were patterned using a 248 nm deep UV stepper, and etched to create strip waveguides, standard rib waveguides (231 nm etch) and ULL Si waveguides with a shallow (56 nm) etch depth. III-V epitaxial material was wafer bonded to the patterned SOI wafers and the InP substrate was removed before wafer-scale processing of the III-V material to provide the hybrid (III-V/Si) gain elements. Processing was finished with encapsulation and metallization to provide completed ICTL devices.

The gain element is 2.5 mm in length, a hybrid Si/III-V waveguide with a Si width of 850 nm to optimize the optical field distribution in the Si and III-V multiple quantum well (MQW) material for low loss and overall high gain. The MQW material includes three InAlGaAs wells, which provides a -3 dB gain bandwidth of $\sim$69 nm; detailed design and performance is described in [24]. Transitions from the hybrid Si/III-V gain section to the passive Si waveguides utilize tapers [24], [25] with approximately 0.5 dB loss per transition and -33 dB reflections.

The mask layout for the three ring ICTL device, a photograph of the device used for results in this paper, and a photograph of a device being probed in the measurement setup are shown in Fig. 5. The fabricated ICTL device includes a tunable reflector to the left of the gain element, the output of which is partly

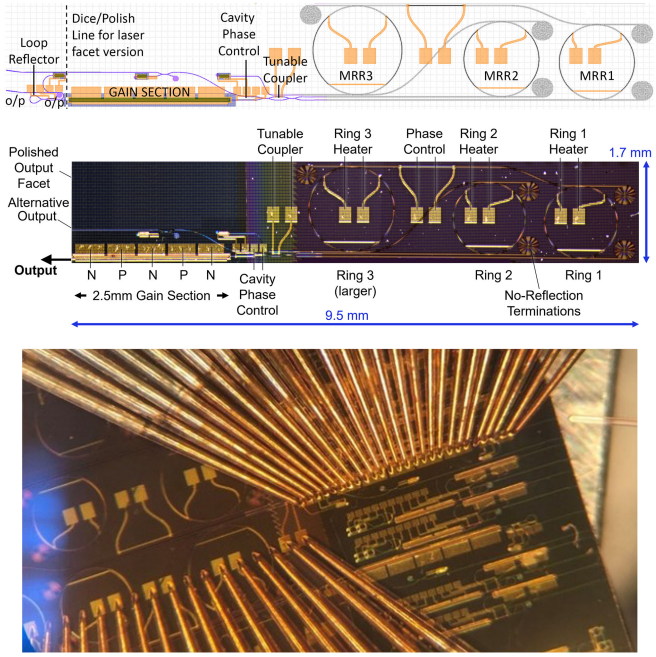

Fig. 5. Layout of 3 ring ICTL with large probe pads and dice mark (top), labelled photo of ICTL device (middle), probed ICTL device (bottom).

coupled to a monitor photodiode before the rest of the power is output from an angled tapered waveguide. Initial measurements were carried out using this geometry, however, to improve phase noise/linewidth performance, the loop reflector and additional elements were diced off and the Si waveguide polished to provide a natural facet reflectivity, R$\sim$ 0.32. The device photograph in the center of Fig. 5 is of the ICTL after this facet polish. The gain element includes five enlarged bond pads (contacting N : P : N : P : N regions of the gain material) for improved heatsinking over previous designs. The cavity phase control, used in the experiments, is a heater next to a Si rib waveguide, and the overall chip size is 9.5 mm x 1.7 mm.

IV. ICTL Measurements

An ICTL tuning map was obtained by scanning resonance frequencies (heater powers) of two MRRs (51 values each), leaving the other unbiased, at each pair of MRR powers scanning the cavity phase (21 values) to maximize the output power. When optical spectra confirmed singlemode operation with side mode suppression Ratio (SMSR) $>$30 dB, the bias powers were stored to file with wavelength, SMSR, and power, without any further optimization of heater settings. An example of this tuning scan for 300 mA bias is shown in Fig. 6. Resonances of the two similar rings, MRR 1 and MRR 2, are close enough across a small wavelength range for lasing once the third ring, MRR 3, is tuned to the same resonance frequencies, e.g., for MRR 2 zero power, when MRR 3 is scanned across its complete range, the laser wavelength is tuned between 1520 and 1530 nm. As the MRR 2 heater power is increased, this lasing wavelength range moves to shorter wavelengths, i.e., $\sim$1510 nm for 20 mW heater power, with the minimum wavelength near 1490 nm (40 mW heater), before lasing wavelengths jump to long wavelength near

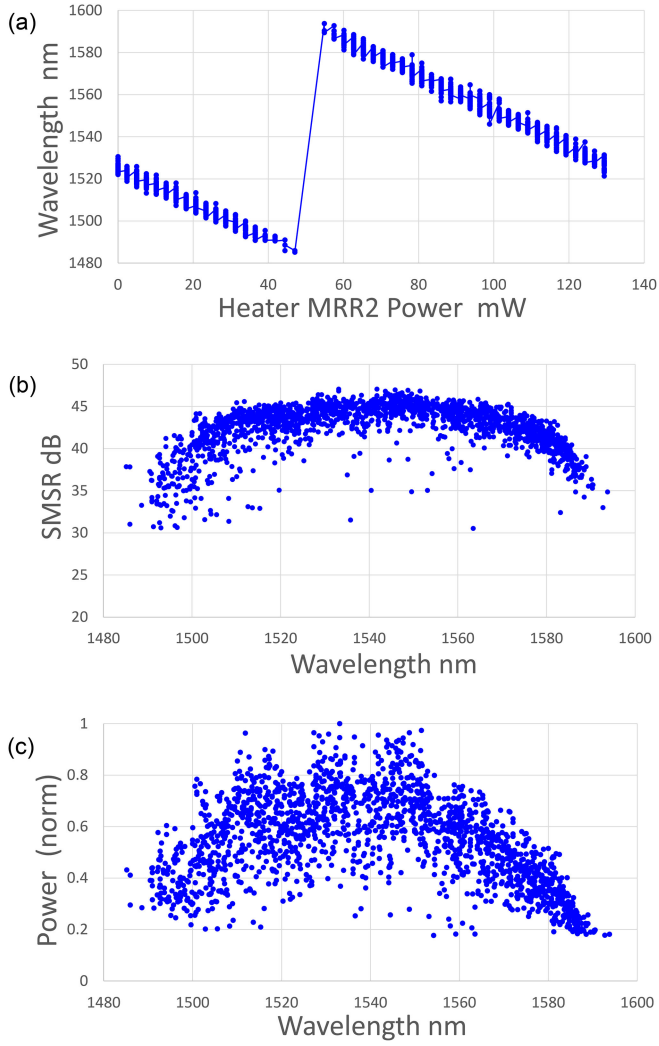

Fig. 6. (a) Heater tuning scan (300mA), (b) SMSR, (c) Power vs. wavelength.

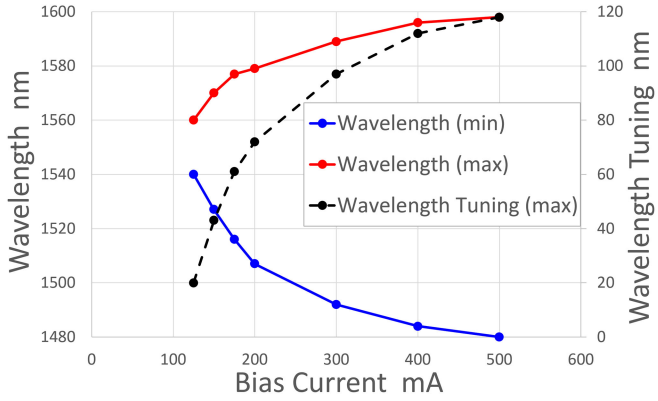

Fig. 7. Heater scans showing wavelength tuning extremes (minima and maxima), plus total tuning range versus gain element bias current.

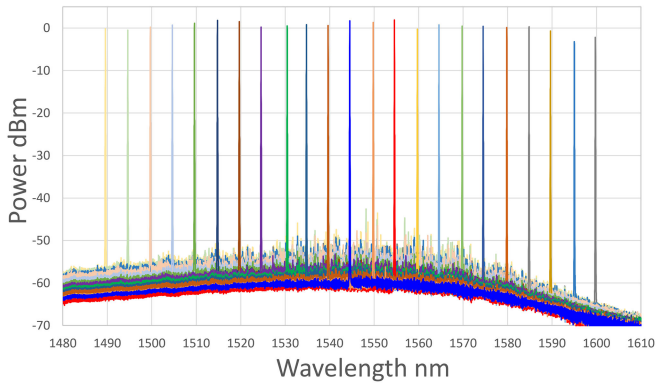

Fig. 8. Various high resolution ICTL spectra (normalized to 1550nm trace).

1590 nm at 60 mW heater power. The gap in lasing points for MRR heater powers between 40 mW and 60 mW reduces as the laser bias current is increased, until the maximum tuning range is found with no gap, e.g., at 500 mA ∼ 118 nm tuning. From the stored data, SMSR (using a large resolution bandwidth for the 120 nm wavelength scans) and normalized power are both plotted versus lasing wavelength in Fig. 6(b), and (c).

The same tuning scan was carried out for a series of bias currents, finding the wavelength tuning range for each bias, while also finding the laser threshold current of ∼125 mA, from where the wavelength tuning rage is smallest; as shown in Fig. 7. A maximum tuning range of 118 nm is found for 500 mA bias, using the tuning points stored to file, and not trying to further optimize bias points to extend the range.

High resolution spectra (0.02 nm RBW) were taken on the ICTL device with the polished facet in order to confirm singlemode operation and measure SMSR. Spectra for lasing wavelengths between 1490 and 1600 nm at a 5 nm spacing are shown in Fig. 8, taken using data from a tuning scan for ring and phase control heater powers. These spectra demonstrate the high fidelity of the laser output. The ICTL device can be continuously tuned across its full 118 nm tuning range using appropriate heater values. The maximum fiber coupled output power seen from these spectra, after a two stage fiber isolator, is 1.54 mW, for operation at 1555 nm, equivalent to ∼15 mW in the output Si strip waveguide, assuming a 10 dB lensed fiber coupling loss.

SMSR values close to the lasing wavelength (i.e., +/− 2 nm) are all above 50 dB, and above 60 dB for operation at longer wavelengths. Operating at the wavelength extremes provides much higher ASE ripple near the gain peak at 1550 nm, reducing the SMSR when considering the full wavelength scan. However, even in that case SMSR is always above 40 dB. SMSR values versus wavelength are summarized in Fig. 9, including points for SMSR close in, and over the full 130 nm measurement range. Fine tuning the MR resonance frequencies and phase control would improve operation and SMSR values at the wavelength extremes, as well as optimizing the central tunable 2:2 coupler to 50/50 for those wavelengths.

Extensive development of the experimental setup was required to measure such low values of FN and Lorentzian linewidth. FN measurements were taken using a commercial OEWaves OE4000 linewidth/phase noise measurement system. The ICTL gain section bias current was provided by a Vescent laser controller (D2-105-500), that includes an ultra-low noise current source. Keithley analog voltage supplies (2200 series) plus screened RC filters (∼ 5 Hz lowpass) were used to drive the

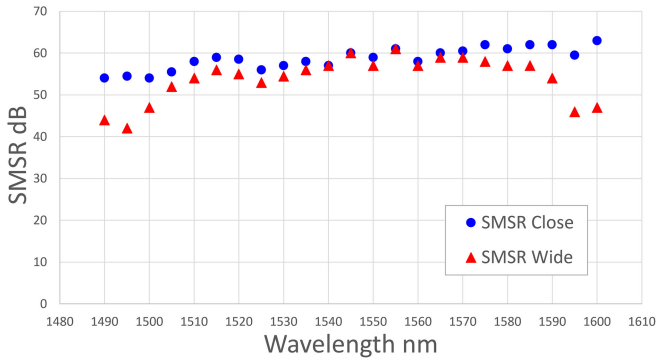

Fig. 9. Lasing mode SMSR (close and wide) versus lasing wavelength.

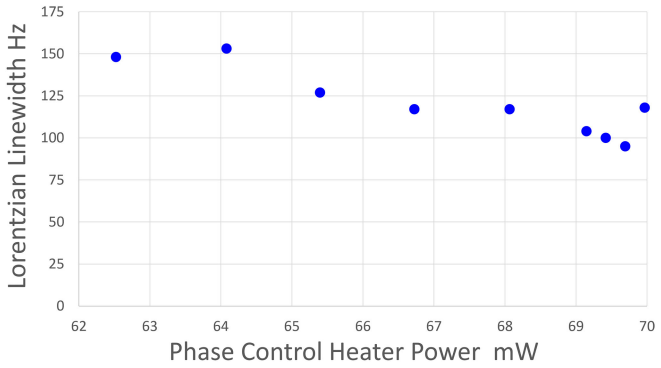

Fig. 11. Lorentzian linewidth, various Phase Control heater powers, 400 mA.

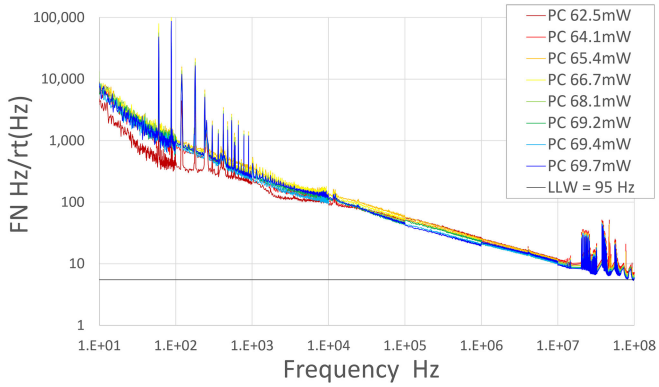

Fig. 10. FN measurements for various Phase Control heater powers, 400 mA.

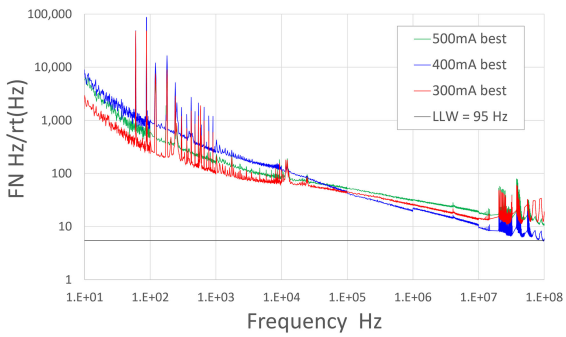

Fig. 12. Best FN measurements at various laser bias currents.

device heaters. A large temperature controlled stage driven by an ILX LDT-5910C unit kept the device temperature constant. Additionally, an aluminum foil coated polystyrene box shielded the whole experiment, to keep out air flow, acoustic pickup, and EMI. An erbium doped fiber amplifier (EDFA) was used to boost the laser power for accurate FN measurements (lowering the OE4000 noise floor), with data taken to confirm that this did not affect FN results. Measurements for the ICTL device with the left side of the gain element polished to provide a natural reflectivity (R $\sim$ 0.32) facet, as shown in Fig. 5, were taken for laser bias currents of 300 mA, 400 mA and 500 mA, in each case varying the cavity phase to move the lasing wavelength to the long wavelength side of the laser reflector and reduce the Lorentzian linewidth through detuned loading [26]. Fig. 10 shows measurements of FN versus frequency for a laser bias of 400 mA and various phase control heater powers. The FN characteristic describes the 1/f or technical noise of the laser at lower frequencies, whereas FN should reach a white noise (flat) floor at higher frequencies, which is associated with the Lorentzian linewidth, or fundamental linewidth, of the laser, i.e., the Lorentzian linewidth is $FN^2.\pi$, using the white noise floor value for FN, or lowest FN value if the floor is not reached.

The best results were obtained at 400 mA bias, as shown in Fig. 10. All of the FN measurements show a long 'tail' out to higher frequencies, which is not typical for a semiconductor laser, e.g., [13]. This extended tail is seen in all E-DBR and ICTL heterogeneously integrated lasers [18], [21], [23], the source of this additional low-frequency FN likely due to carrier trapping at the III-V/Si bonded interface [27]. As FN is still reducing (on the same slope) at the highest measured frequency of 100 MHz, the flat white noise floor has not yet been reached, therefore results indicate that the Lorentzian linewidth is less than the value calculated from this minimum FN value, i.e., less than 95 Hz.

Plotting these Lorentzian linewidths versus phase control heater power in Fig. 11 shows the expected reduction in linewidth as wavelength (detuned loading) increases, with a minimum value of 95 Hz found, a record for an integrated semiconductor tunable laser. The fact that FN is clearly still reducing even at 100 MHz means that the actual Lorentzian linewidth is lower than 95 Hz – this lower value could be found if the FN measurement was extended to higher frequency.

Higher FN was found at 300 mA bias, with an associated Lorentzian linewidth of 410 Hz, obtained at a lower frequency of 30 MHz where the white noise floor was reached. Operation at 500 mA, with higher laser output power than at 400 mA, provided a higher value for Lorentzian linewidth (at 100 MHz) of 360 Hz - whereas a lower linewidth is expected. This increase in Lorentzian linewidth at this highest bias current is likely due to a larger/extended FN tail from the higher current level. FN measurements up to higher frequencies would reach the white noise floor in both the 400 mA and 500 mA bias current cases, and would provide measurements for Lorentzian linewidths that are significantly below those found at 100 MHz. The best FN measurements at each of these three bias current, 300 mA, 400 mA and 500 mA, are included together in Fig. 12. These results provide a good comparison of the long tail of the FN

measurements and how it varies with laser bias current. The lowest FN below 10 kHz is found for 300 mA bias, whereas the largest FN tail, seen above 100 kHz, is found for the highest bias current of 500 mA.

This run of heterogeneously integrated ICTL devices using the improved process steps produced significantly higher power than earlier devices, and no degradation in operation was seen during extensive testing. However, the maximum output power coupled into an optical fiber was only 1.54 mW, when operating at 1555 nm with a 500 mA bias, due to the low coupling efficiency of the polished Si strip waveguide facet to a lensed fiber, which is estimated to provide ∼10 dB coupling loss. This indicates a maximum on chip output power of ∼15 mW. This ICTL device has a polished-back silicon wire waveguide, which is not optimized for coupling. When using an inverse tapered waveguide together with a high numerical aperture fiber (e.g., Nufern UHNA7) a coupling loss closer to 1 dB is possible, which would provide over 10 mW of optical power in the output fiber. This level of optical power is acceptable in many system applications, especially those that incorporate an EDFA, such as in telecom systems.

The threshold current found from tuning scans (Fig. 7) was found to be relatively high, ∼125 mA. It is believed that the excellent loss characteristics measured for passive ULL silicon waveguides in [20] were degraded by subsequent wafer bonding and III-V processing, leading to higher threshold current and lower output power than expected, due to the long cavity length (108 mm) with increased loss. Future devices will include additional processes to protect the ULL Si waveguides during later processing steps and to preserve the passive waveguide loss in the final devices. This will significantly reduce threshold currents and increase output powers of the ICTL devices, as well as further reduce low frequency FN and Lorentzian linewidth.

For applications such as interferometric acoustic sensing systems that require even lower FN at low frequencies, where 1/f type technical noise dominates (e.g., see Figs. 10 and 12), frequency locking the laser to a reference resonator using Pound Drever Hall (PDH) based electronic feedback [28] can significantly reduce FN. Recent results from a hybrid integrated E-DBR laser [13] and a long (4 meter) Silicon Photonics foundry based integrated coil resonator demonstrated FN < 0.5 Hz/(Hz)$^{0.5}$ at 10 kHz, well below the free running laser response [29]. Such an MRR based integrated resonator with wideband operation could be used with, or integrated with, an ultra-wideband tunable laser such as the ICTL.

RIN measurements were made at 500 mA bias current, 1550 nm operation with 1.2 mW optical power from the ICTL into the measurement system. Results were taken both with and without an EDFA, from 1 to 20 GHz, and these measurements are shown in Fig. 13.

Without the EDFA, the RIN reaches a minimum of approximately −160 dBc/Hz at 3 GHz, peaking at 8 to 12 GHz, then rising above 15 GHz. The measurement noise floor comes from both photodetector thermal noise and the spectrum analyzer noise floor - due to the low optical input power level. Adding an EDFA and operating at higher optical power into the photodetector (∼ 10 mW) improves the RIN values in most cases

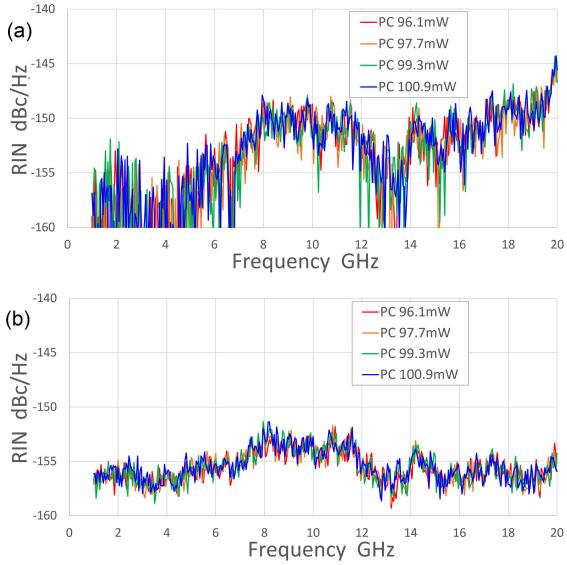

Fig. 13. RIN vs. phase control heater power (a) No EDFA, (b) With EDFA.

(except near 3 GHz), with an optimistic EDFA noise figure (NF) of 5 dB added to measured values, providing worst case RIN of approximately −155 dBc/Hz, the RIN value being below that over most of that frequency range, with a broad peak near −155 dBc/Hz from 8 to 12 GHz.

V. Conclusion

The operating principles and design process of the novel ICTL device, incorporating three or more large, ultra-low loss MRRs in a Sagnac loop based laser reflector, have been described. The ICTL provides ultra-wideband wavelength tuning with ultralow noise performance. An ICTL device incorporating an ultra-low loss Si based laser reflector, fabricated with heterogeneous integration of a III-V gain element on the Silicon Photonics platform, is demonstrated to provide a record 118 nm of continuous wavelength tuning and Lorentzian linewidth below 95 Hz. The ICTL has worst case laser RIN of −155 dBc/Hz, at a maximum on-chip optical power of ∼15 mW. This Silicon Photonics Foundry-ready integrated laser device provides performance that will be disruptive for many photonic applications.

Acknowledgment

The views and conclusions in this paper are those of the authors and should not be interpreted as presenting official policies or position. The U.S. Government is authorized to reproduce and distribute reprints.

References

[1] J. Yao, "Microwave photonics: Photonic generation of microwave and millimeter-wave signals," *Int. J. Microw. Opt. Technol.*, vol. 5, no. 1, 2010, Art. no. 16.

[2] F. Hamaoka *et al.*, "Ultra-wideband WDM transmission in S-, C-, and L-bands using signal power optimization scheme," *J. Lightw. Technol.*, vol. 37, no. 8, pp. 1764–1771, Apr. 2019.

[3] C. V. Poulton *et al.*, "Long-range LiDAR and free-space data communication with high-performance optical phased arrays," *IEEE J. Sel. Topics Quantum Electron.*, vol. 25, no. 5, Sep./Oct. 2019, Art. no. 7700108.
[4] P. A. Morton *et al.*, "Integrated coherent tunable laser (ICTL) with 118 nm tuning range and sub-100 Hz lorentzian linewidth," in *Proc. Opt. Fiber Commun. Conf.*, 2021, Art. no. TuG2.1.
[5] T. Komljenovic *et al.*, "Photonic integrated circuits using heterogeneous integration on silicon," *Proc. IEEE*, vol. 106, no. 12, pp. 2246–2257, Dec. 2018.
[6] N. Margalit, C. Xiang, S. M. Bowers, A. Bjorlin, R. Blum, and J. E. Bowers, "Perspective on the future of silicon photonics and electronics," *Appl. Phys. Lett.*, vol. 118, no. 22, May 2021, Art. no. 220501.
[7] T. Segawa, S. Matsuo, T. Kakitsuka, T. Sato, Y. Kondo, and H. Suzuki, "Full C-band tuning operation of semiconductor double-ring resonator-coupled laser with low tuning current," *IEEE Photon. Technol. Lett.*, vol. 19, no. 17, pp. 1322–1324, Sep. 2007.
[8] S. Matsuo and T. Segawa, "Microring-resonator-based widely tunable lasers," *IEEE J. Sel. Topics Quantum Electron.*, vol. 15, no. 3, pp. 545–554, May/Jun. 2009.
[9] T. C. Nobuhide and M. Ishizaka, "Compact, lower-power-consumption wavelength tunable laser fabricated with silicon photonic-wire waveguide micro-ring resonators," *Opt. Exp.*, vol. 17, no. 16, 2009, Art. no. 14063.
[10] R. M. Oldenbeuving *et al.*, "25 kHz narrow spectral bandwidth of a wavelength tunable diode laser with a short waveguide-based external cavity," *Laser Phys. Lett.*, vol. 10, 2013, Art. no. 1.
[11] J. C. Hulme, J. K. Doylend, and J. E. Bowers, "Widely tunable vernier ring laser on hybrid silicon," *Opt. Exp.*, vol. 21. 2013, Art. no. 19718.
[12] C. Xiang *et al.*, "Effects of nonlinear loss in high-Q si ring resonators for narrow-linewidth III-V/Si heterogeneously integrated tunable lasers," *Opt. Exp.*, vol. 28, no. 14, 2020, Art. no. 19926.
[13] P. A. Morton *et al.*, "High-power, ultra-low noise hybrid lasers for microwave photonics and optical sensing," *J. Lightw. Technol.*, vol. 36, no. 21, pp. 5048–5057, Nov. 2018.
[14] Thorlabs Single-Frequency, Ultra-Low-Noise (ULN) laser, [Online]. Available: https://www.thorlabs.com/newgrouppage9.cfm?objectgroup_id=13653
[15] P. Morton, J. Khurgin, and C. Morton, "Multiple-microresonator based laser," U.S. Patents 9,559,484, and 9,748,726, 2017.
[16] J. Zhang *et al.*, "III-V-on-Si photonic integrated circuits realized using micro-transfer-printing," *APL Photon.*, vol. 4, no. 11, Nov. 2019, Art. no. 110803.
[17] C. Xiang, Paul A. Morton, J. Khurgin, C. Morton, J. E. Bowers *et al.*, "Widely tunable Si_3N_4 triple-ring and quad-ring resonator laser reflectors and filters," in *Proc. IEEE 15th Int. Conf. Group IV Photon.*, 2018, pp. 1-2.
[18] C. Xiang *et al.*, "Narrow-linewidth III-V/Si/Si_3N_4 laser using multilayer heterogeneous integration," *Optica*, vol. 7, no. 1, pp. 20–21, 2020.
[19] C. Xiang *et al.*, "High-performance lasers for fully integrated silicon nitride photonics," *Nature Commun.*, vol. 12, no. 1, pp. 1–8, 2021.
[20] M. Tran *et al.*, "Ultra-Low-Loss silicon waveguides for heterogeneously integrated Silicon/III-V photonics," *Appl. Sci.*, vol. 8, 2018, Art. no. 1139.
[21] D. Huang *et al.*, "High-power sub-kHz linewidth lasers fully integrated on silicon," *Optica*, vol. 6, no. 6, pp. 745–752, 2019.
[22] A. Zilkie *et al.*, "Multi-Micron silicon photonics platform for highly manufacturable and versatile PICs," *IEEE J. Sel. Topics Quantum Electron.*, vol. 25, no. 5, Sep./Oct. 2019, Art. no. 8200713.
[23] M. Tran *et al.*, "Ultra-low noise widely-tunable semiconductor lasers fully integrated on silicon," in *Proc. IEEE Comp. Semi. Week*, 2019, pp. 1–2.
[24] M. L. Davenport, S. Skendžić, N. Volet, J. C. Hulme, M. J. R. Heck, and J. E. Bowers, "Heterogeneous silicon/III-V semiconductor optical amplifiers," *IEEE J. Sel. Top. Quantum Electron.*, vol. 22, no. 6, Nov./Dec. 2016, Art. no. 3100111.
[25] M. L. Davenport *et al.*, "Heterogeneous integration of III–V lasers on SI by bonding," *Semiconductors Semimetals*, vol. 99, pp. 139–188, 2018.
[26] K. Vahala *et al.*, "Detuned loading in coupled cavity semiconductor lasers-Effect on quantum noise and dynamics," *Appl. Phys. Lett.*, vol. 45, no. 5, 1984, Art. no. 501.
[27] A. Van Der Ziel, "Unified presentation of 1/f noise in electronic devices: Fundamental l/f noise sources," *Proc. IEEE*, vol. 76, no. 3, pp. 233–258, Mar. 1988.
[28] R. W. P. Drever *et al.*, "Laser phase and frequency stabilization using an optical resonator," *Appl. Phys. B*, vol. 31, pp. 97–105, 1983.
[29] K. Liu *et al.*, "Precision laser stabilization using photonic integrated coil resonator," in *Proc. OSA Front. Opt. Laser Sci.*, 2021, Art. no. FTh2A.1.

Paul A. Morton (Fellow, IEEE) was born in Stockton-on-Tees, England. He received the B.Sc., M.Eng. and Ph.D. degrees in electrical engineering from the University of Bath, Bath, U.K.

As a Researcher with AT&T Bell Laboratories he made fundamental research contributions in the areas of high-speed laser diodes, mode-locked optical pulse-sources, and photonic integration. At Ciena corporation, he was a Technical Leader in the development of commercial high capacity DWDM transmission systems. In 2002, Dr. Morton is the Co-Founded Morton Photonics, a technology company focused on research and development of advanced photonic technologies. In recent years, he has focused on photonic components and photonic integrated circuits (PICs) on the silicon photonics platform, and subsystems for applications of high performance analog RF Photonic links, sensing, photonic processing for phased array systems, and transitioning these devices to commercial and DoD systems. Dr. Morton is a Fellow of the Optical Society of America.

Chao Xiang received the B.E. degree in optoelectronic information engineering from the Huazhong University of Science and Technology, Wuhan, China, the M.Phil. degree in information engineering from the Chinese University of Hong Kong, Hong Kong, and the Ph.D. degree with the Department of Electrical and Computer Engineering from the University of California, Santa Barbara, CA, USA. He is currently a Postdoctoral Scholar with the University of California, Santa Barbara, CA, USA. His research interests include semiconductor lasers, heterogeneous photonic integration, and integrated nonlinear photonics and photonic integrated circuits.

Jacob B. Khurgin received the M.S. degree in optics from the Institute of Fine Mechanics and Optics (ITMO), St Petersburg, Russia, in 1979. In 1980, he emigrated to US, and joined Philips Laboratories in Briarcliff Manor, NY, USA. There for 8 years he worked on miniature lasers, II-VI semiconductor lasers, various display and lighting fixtures, and small appliances. Simultaneously he was working toward his Graduate studies with the Polytechnic Institute of NY, where he received the Ph.D. degree in electro-physics in January 1987. In January 1988, he joined the ECE Department of Johns Hopkins University, where he is currently a Professor. His research topics over the years included an eclectic mixture of optics of semiconductor nanostructures, nonlinear optical devices, semiconductor lasers, optical communications, plasmonics, laser refrigeration, microwave photonics, opto-mechanics, and condensed matter physics. He is a Fellow of OSA and APS.

Christopher D. Morton biography is not available at the time of publication.

Minh Tran biography is not available at the time of publication.

Jon Peters biography is not available at the time of publication.

Joel Guo biography is not available at the time of publication.

Michael J. Morton biography is not available at the time of publication.

John E. Bowers (Fellow, IEEE) received the M.S. and Ph.D. degrees from Stanford University, Stanford, CA, USA. He is the Director of the Institute for Energy Efficiency and a Professor with the Departments of Electrical and Computer Engineering and Materials, the University of California, Santa Barbara, CA, USA. His research interests primarily concerned with silicon photonics, optoelectronic devices, optical switching and transparent optical networks and quantum dot lasers. He worked for AT&T Bell Laboratories and Honeywell before joining UCSB. Bowers is a Fellow of OSA and the American Physical Society, and was the recipient of the IEEE Photonics Award, OSA/IEEE Tyndall Award, the IEEE LEOS William Streifer Award and the South Coast Business and Technology Entrepreneur of the Year Award. He is a member of the National Academy of Engineering and the National Academy of Inventors.